



Temporally quasiperiodic data, propagating in the laboratory frame, can be rendered periodic by Galilean transformation

Bill D. Caraway  and Arne J. Pearlstein *

Department of Mechanical Science and Engineering, University of Illinois at Urbana-Champaign, 1206 West Green Street, Urbana, Illinois 61801, USA



(Received 6 October 2021; accepted 6 July 2022; published 9 August 2022)

For a broad class of distributions of temperature, concentration, or another quantity propagating rectilinearly, we show that temporally quasiperiodic behavior in the laboratory frame can be rendered periodic by Galilean transformation. The approach is illustrated analytically and numerically using as an example a closed-form model distribution generated from a one-dimensional partial differential equation, and a detailed process is developed to determine frame speed from more general quasiperiodic, one-dimensional, temporally- and spatially-discretized data. The approach is extended to two- and three-dimensional rectilinear propagation, and its application to nonrectilinear propagation, along with implications for interpreting noise-corrupted data, are also discussed.

DOI: [10.1103/PhysRevE.106.024607](https://doi.org/10.1103/PhysRevE.106.024607)

I. INTRODUCTION

In many systems, spatiotemporal variation propagates through a medium. In some cases, data are acquired as time series at fixed locations. Examples include temperature fields in moving fluids sensed by thermocouples [1,2]; concentration distributions in moving fluids sensed electrochemically [3]; velocity fields sensed using hot-wire, hot-film, laser-Döppler, or electrochemical techniques [4–6]; and acoustic waves sensed by pressure or velocity microphones [7]. In other cases, data can be acquired by moving a sensor along a line or other path [8]. Data can also be acquired continuously or nearly continuously in space and time (frequently optically) in systems involving flow [9–16] or involving wave propagation either in nominally motionless chemically reacting systems [17–26] or in rings of cardiac cells [27,28].

In all of these cases, data are typically analyzed in the laboratory frame. When a preferred direction exists (e.g., due to mean fluid flow, in situations involving rotating waves in a plane [27,28], and in other wave propagation through a quiescent medium), the question arises as to whether one can gain additional insight, or simplify analysis of data, by considering the data in a different reference frame. In some cases, it is known that the answer is “yes.” Examples include use of Galilean transformations to identify vortices and other propagating structures in shear-flow experiments and computations [29,30]. More recently, a non-Galilean transformation has been employed to obtain a first-order ordinary differential equation used to analyze time-dependent experimental data for motion of the rim bounding a decelerating liquid sheet resulting from drop impact on a solid surface [31]. From the standpoint of theory, transformation to a moving frame has been used to analyze traveling-wave phenomena in a wide range of applications [32–38].

Here we consider whether experimental data or computational results exhibiting temporal quasiperiodicity and propagation in the laboratory frame [23,24,39–40] can be rendered time periodic by a change of frame and, if so, how one identifies the frame transformation. That such a transformation is sometimes possible is illustrated by a simple example. Consider a medium at rest in which oscillating chemical reaction generates time-periodic concentration distributions in the form of standing or rotating waves with temporal frequency f_{chem} . Now suppose that the medium is rotated with angular velocity $\Omega = 2\pi f_{\text{rot}}$, with f_{chem} and f_{rot} incommensurable. To a laboratory-frame observer, concentrations at any point will be temporally quasiperiodic [41], even though the underlying chemical dynamics are strictly time periodic. Transformation to a frame rotating with the medium will clearly render the distributions time periodic.

Can this simple result for azimuthal propagation in a plane be extended to rectilinear and other propagation if the geometry is not periodic? For a broad class of temporally quasiperiodic distributions (possibly after an initial transient) depending on a Cartesian coordinate η and time τ through precisely two distinct linear combinations of those variables, we answer affirmatively, by showing that Galilean transformation renders such distributions time periodic. We show how to determine appropriate reference frames, and that the approach is directly extendable to some distributions propagating rectilinearly or nonrectilinearly in two and three dimensions, or depending periodically on more linear combinations of the spatial coordinate(s) and time.

The remainder of the paper is organized as follows. In Sec. II, we use a one-dimensional partial differential equation (PDE) to generate model rectilinearly-propagating spatiotemporal distributions, temporally quasiperiodic in the laboratory frame. We show how these example distributions are rendered time periodic in a moving frame by Galilean transformation in Sec. III A, and that the procedure is applicable to a broad class of temporally quasiperiodic distributions in Sec. III B,

*ajp@illinois.edu

where we provide a theoretical foundation. In Sec. III C, we describe in detail how an appropriate frame velocity can be determined for temporally- and spatially-discretized experimental, observational, or computational data. We apply the technique to numerical data in Sec. III D, and generalize to two- and three-dimensional distributions and to nonrectilinear propagation in Sec. IV, followed by a discussion, including effects of noise, and conclusions in Sec. V.

II. MODEL DISTRIBUTIONS

A. Generation of model distributions

We illustrate the process for transforming laboratory-frame quasiperiodicity to moving-frame periodicity using example distributions generated by closed-form solution of initial boundary-value problems for the linear PDE:

$$\frac{\partial u}{\partial \tau} = \sigma \frac{\partial(Gu)}{\partial \eta}, \quad (1)$$

with $G(\eta, \tau) = \cos(2\pi\tau - 2\pi\mu\eta)$, where the amplitude σ and wavenumber μ are positive and the forcing frequency is unity. The linear PDE (1) arises in the limit of negligible Fickian diffusion in a dimensionless model of high-frequency

pressure-wave effects on concentration distributions in a quiescent binary liquid solution [42]. Here, we simply use it to generate model propagating distributions $u(\eta, \tau)$ quasiperiodic in time.

Closed-form solutions of (1) are obtained using the method of characteristics. We restrict consideration to an unbounded domain and $\sigma\mu < 1$, and denote the initial condition $u(\eta, 0)$ by $u_0(\eta)$. Introducing characteristic variables α and β defined by $\partial\tau(\alpha, \beta)/\partial\beta = 1$ and

$$\frac{\partial\eta(\alpha, \beta)}{\partial\beta} = -\sigma G(\eta, \tau) = -\sigma \cos(2\pi\tau - 2\pi\mu\eta), \quad (2)$$

subject to initial conditions $\tau(\alpha, 0) = 0$ and $\eta(\alpha, 0) = \alpha$, we rewrite (1) and its initial condition as

$$\begin{aligned} \frac{\partial\tilde{u}(\alpha, \beta)}{\partial\beta} &= \frac{\partial\tau}{\partial\beta} \frac{\partial\tilde{u}}{\partial\tau} + \frac{\partial\eta}{\partial\beta} \frac{\partial\tilde{u}}{\partial\eta} \\ &= \sigma \frac{\partial G(\eta, \tau)}{\partial\eta} \tilde{u} = 2\pi\sigma\mu \sin(2\pi\tau - 2\pi\mu\eta) \tilde{u} \end{aligned} \quad (3)$$

and $\tilde{u}(\alpha, 0) = \tilde{u}_0(\alpha)$, respectively, where $\tilde{u}(\alpha, \beta) = u(\eta(\alpha, \beta), \tau(\alpha, \beta))$. We define $\kappa \equiv \sigma\mu$, and solve for $\tau(\alpha, \beta)$ and $\eta(\alpha, \beta)$ subject to the initial conditions, obtaining $\tau(\alpha, \beta) = \beta$ and

$$\eta(\alpha, \beta) = \frac{1}{\mu} \left[\beta + \frac{1}{\pi} \arctan \left(\frac{\omega \tan(\pi\mu\alpha) - (1 + \kappa) \tan(\pi\omega\beta)}{(1 - \kappa) \tan(\pi\mu\alpha) \tan(\pi\omega\beta) + \omega} \right) - \lfloor \omega\beta + \chi(\alpha) \rfloor + \lfloor \mu\alpha \rfloor \right], \quad (4)$$

where $0 < \omega \equiv (1 - \kappa^2)^{1/2} < 1$, $\lfloor \Lambda \rfloor$ is the largest integer not exceeding the real number Λ , and

$$\chi(\alpha) = \begin{cases} 1/2, & \tan(\pi\mu\alpha) = 0 \\ \frac{1}{\pi} \arctan \frac{\omega \cot(\pi\mu\alpha)}{1 - \kappa}, & \tan(\pi\mu\alpha) \neq 0 \end{cases} \quad (5)$$

For integer values of $\omega\beta + \chi(\alpha)$, i.e., when $\omega\beta + \chi(\alpha) = \lfloor \omega\beta + \chi(\alpha) \rfloor$, we take the argument of arctan in (4) to be infinity. Because the right-hand side (RHS) of (4) must be continuous, the last two terms of the second factor of the RHS constitute a piecewise-constant integer-valued function with discontinuities at the nonremovable singularities of the argument of arctan.

Using $\tau(\alpha, \beta) = \beta$ and (4), we solve (3) subject to its initial condition, obtaining

$$\tilde{u}(\alpha, \beta) = \tilde{u}_0(\alpha) \frac{\kappa \cos(2\pi\mu\alpha) - \kappa\omega \sin(2\pi\mu\alpha) \sin(2\pi\omega\beta) - \kappa[\kappa + \cos(2\pi\mu\alpha)] \cos(2\pi\omega\beta) + 1}{\omega^2}. \quad (6)$$

For periodic initial conditions with the wavelength of $G(\eta, \tau)$, i.e., $u_0(\eta) = u_0(\eta + 1/\mu)$, (4) and (6) can be combined as

$$u(\eta, \tau) = \frac{\omega^2 u_0 \left\{ \frac{1}{\pi\mu} \arctan \left[\frac{(1 + \kappa) \tan(\pi\omega\tau) - \omega \tan(\pi\tau - \pi\mu\eta)}{(1 - \kappa) \tan(\pi\omega\tau) \tan(\pi\tau - \pi\mu\eta) + \omega} \right] \right\}}{1 - \kappa [\cos(2\pi\omega\tau) - 1] \cos(2\pi\tau - 2\pi\mu\eta) - \kappa^2 \cos(2\pi\omega\tau) - \kappa\omega \sin(2\pi\omega\tau) \sin(2\pi\tau - 2\pi\mu\eta)}. \quad (7)$$

Solutions for arbitrary initial conditions $u(\eta, 0)$ have closely related structure (see Supplemental Material Sec. A [43] for derivation). For the purpose of generating model quasiperiodic distributions, we restrict consideration to uniform initial conditions.

B. Behavior of model distributions

The distribution $u(\eta, \tau)$ has two principal attributes: oscillation and propagation. Oscillation is evident from the

structure of $u(\eta, \tau)$ or the periodic dependence of $\tilde{u}(\alpha, \beta)$ on β . Propagation is evident from the ‘‘preferred direction’’ of the characteristics, i.e., $\eta(\alpha, \beta + \Delta\beta) > \eta(\alpha, \beta)$ for all sufficiently large $\Delta\beta$. These attributes result in the η - τ periodicity relationships

$$\eta(\alpha, \beta) = \eta(\alpha, \beta + 1/\omega) - (1 - \omega)/(\mu\omega), \quad (8a)$$

$$\tilde{u}(\alpha, \beta) = \tilde{u}(\alpha, \beta + 1/\omega), \quad (8b)$$

$$u(\eta, \tau) = u(\eta + (1 - \omega)/(\mu\omega), \tau + 1/\omega), \quad (8c)$$

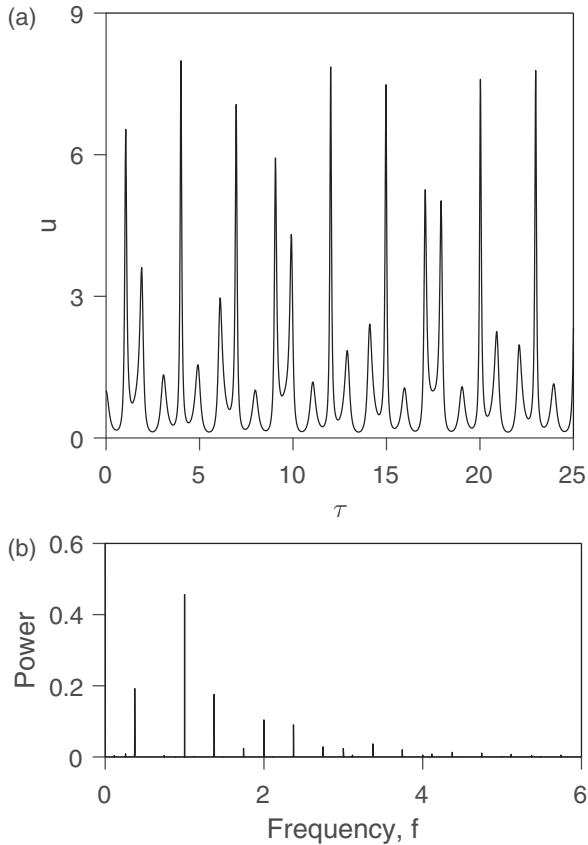


FIG. 1. (a) Time series and (b) power spectrum (arbitrary units) for quasiperiodic response $u(\eta = 0.4, \tau)$ with an intrinsic frequency $\omega = \pi/5$ (incommensurable with the extrinsic frequency 1), $\mu = 10$, and $u_0(\eta) = 1$. In the power spectrum (from a time series over $0 \leq \tau \leq 1000$ sampled uniformly with time increment 10^{-3}), power levels, in arbitrary units, of 1 and 2.79×10^{-4} at $f = 0$ and 6, respectively, are omitted for graphical clarity.

which show that, at each position and time, the value of u is translated from a smaller η at an earlier time. (Recall that $0 < \omega < 1$.)

For irrational ω , (7) shows that a uniform $u_0(\eta)$ gives a $u(\eta, \tau)$ temporally quasiperiodic at each η , and that this $u(\eta, \tau)$ can be written in terms of periodic functions with exactly two specified incommensurable temporal frequencies (unity and ω ; see below). (By “specified,” we refer to the incommensurable frequencies of explicit periodic functions summed, multiplied, divided, exponentiated, etc., to form a closed-form representation of a quasiperiodic function.) The extrinsic frequency, unity, is the PDE’s forcing frequency, while ω is intrinsic to $u(\eta, \tau)$, which is time periodic if ω is rational and quasiperiodic otherwise. For $\omega = \pi/5$, a fixed- η time series [Fig. 1(a)] shows that $u(\eta, \tau)$ is not periodic, and a power spectrum [Fig. 1(b)] confirms quasiperiodicity. As expected, the frequencies in Fig. 1(b) with sensible power, which we refer to as “observed frequencies,” are linear combinations of the specified incommensurable frequencies unity and ω , with integer coefficients (see Supplemental Material Sec. B [43] for supporting table). In what follows, references to linear combinations of incommensurable frequencies are understood to mean linear combinations with integer coefficients.

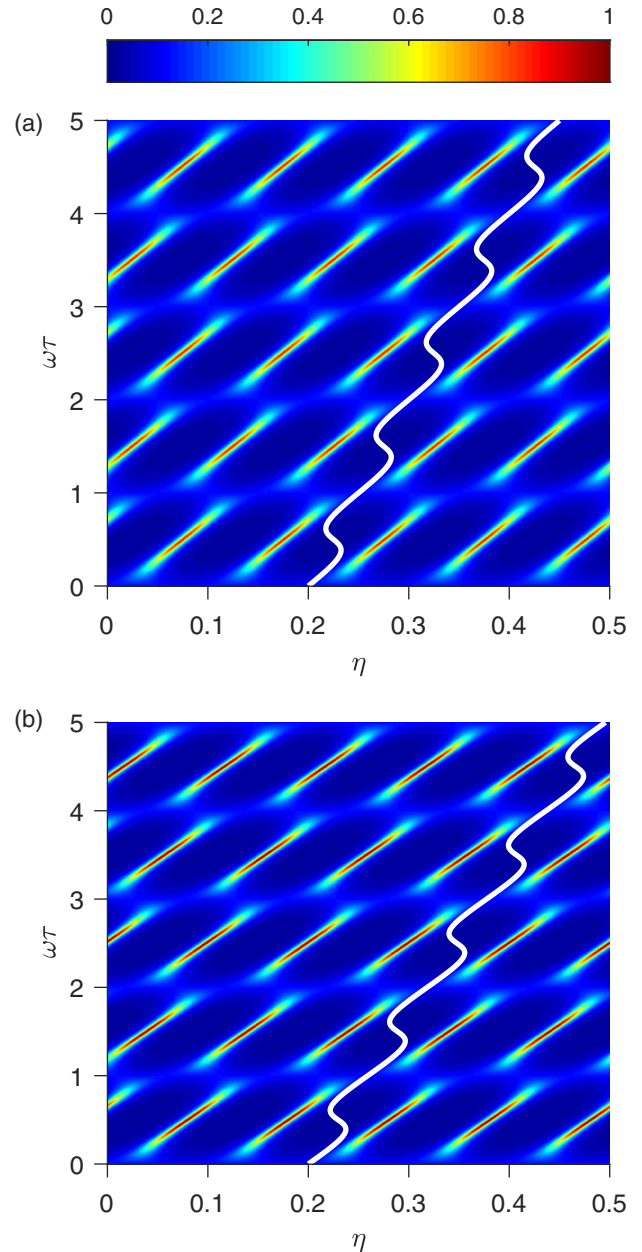


FIG. 2. Variation of $u(\eta, \tau)$ with $\mu = 10$ and $u_0(\eta) = 1$ for two values of the intrinsic frequency: (a) a commensurable case with $\omega = 2/3$ producing periodic response, and (b) an incommensurable case with $\omega = \pi/5$ producing quasiperiodic response. The $\alpha = 0.2$ characteristic is shown as a continuous white curve. $u(\eta, \tau)$ has been scaled by $8.007 = \max[u(\eta, \tau; \omega = \pi/5)] > \max[u(\eta, \tau; \omega = 2/3)]$.

The η - τ plane can be divided into temporal intervals of duration $1/\omega$, during each of which $u(\eta, \tau)$ is directly translatable from the preceding interval at the location $\eta - (1-\omega)/(\mu\omega)$ [see (8a)–(8c)]. As shown in Figs. 2(a) and 2(b), each temporal interval includes a spatially periodic set of high-amplitude spatiotemporal “ridges.” As ω increases, the ridge amplitude decreases and the angle of inclination in the η - τ plane increases. From (8a)–(8c), it is seen that periodicity obtains only if ω is rational. Otherwise, no number

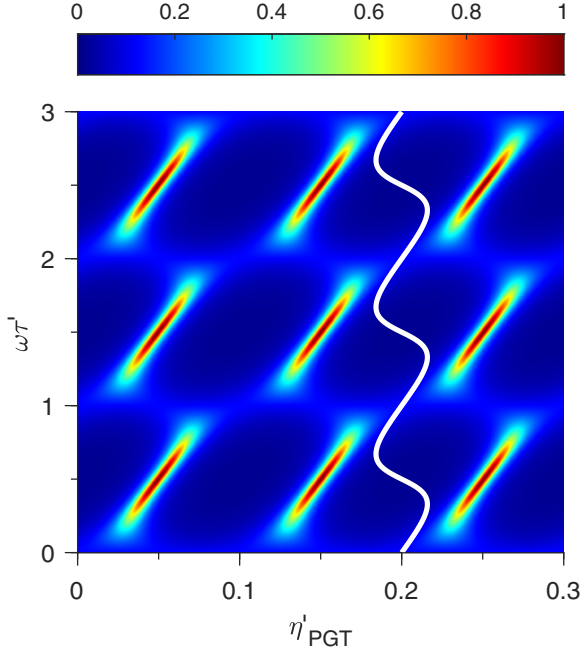


FIG. 3. Spatiotemporal variation of $U(\eta'_{\text{PGT}}, \tau')$, with intrinsic frequency $\omega = \pi/5$ (incommensurable with the extrinsic frequency 1), $\mu = 10$, and $u_0(\eta) = 1$ [case shown in Fig. 2(b)], with magnitude scaled by $8.007 = \max[U(\eta'_{\text{PGT}}, \tau')]$. In this PGT frame, the $\alpha = 0.2$ characteristic is shown as a continuous solid white curve and is time periodic.

of temporal intervals will produce a cumulative η shift that is an integer multiple of $1/\mu$, the wavelength of $u(\eta, \tau)$.

III. GALILEAN TRANSFORMATIONS

A. Galilean transformation of model distributions

For uniform initial conditions, (7) shows that the one-dimensional $u(\eta, \tau)$ can be written in closed form using time-periodic functions with two distinct arguments, $\omega\tau$ and $\tau - \mu\eta$. The “primary” Galilean transformation (PGT) and corresponding frame velocity

$$\eta'_{\text{PGT}} = \eta - v_{\text{PGT}}\tau, \quad (9a)$$

$$\tau' = \tau, \quad (9b)$$

$$v_{\text{PGT}} = (1 - \omega)/\mu, \quad (9c)$$

collapse the two frequencies of the laboratory-frame $u(\eta, \tau)$ to the single-frequency ω of the moving-frame distribution $U(\eta'_{\text{PGT}}, \tau') \equiv u(\eta'_{\text{PGT}} + v_{\text{PGT}}\tau', \tau') = u(\eta, \tau)$, where η'_{PGT} is the spatial coordinate in the moving frame. (In Sec. III B, we describe the underlying theory. In Sec. III C, we discuss how to determine an appropriate Galilean transformation from temporally- and spatially-discretized data when the functional form of the distribution is unknown. In Sec. IV, we extend this approach to additional spatial dimensions and greater spatiotemporal complexity.) Figure 3 illustrates the spatiotemporal behavior of $U(\eta'_{\text{PGT}}, \tau')$ in the PGT frame.

Periodic dependence of η'_{PGT} on β (Fig. 3) indicates that v_{PGT} matches the time-averaged propagation speed of $u(\eta, \tau)$, making the transformed distribution $U(\eta'_{\text{PGT}}, \tau')$ time periodic for any ω . This is consistent with the characteristics (i.e.,

η'_{PGT} as a function of β for given α) being time periodic with the same β periodicity as $\bar{u}(\alpha, \beta)$.

For ω incommensurable with unity, Fig. 4(a) shows that a “moving-frame time series,” constructed from the continuous moving-frame distribution $U(\eta'_{\text{PGT}}, \tau')$, is time periodic with frequency ω . Spectral decay with increasing f is initially approximately linear [Fig. 4(a)], and asymptotically exponential [Fig. 4(b)].

A more general Galilean transformation replaces (9a) by $\eta' = \eta - v\tau$, where for our example distribution it is convenient to write $v = (1 - \gamma)/\mu$ with γ arbitrary. Several choices of γ stand apart. For $\gamma = 0$ or $-\omega$, the transformed distribution is time periodic with specified frequency ω . For $\gamma = k\omega$ ($|k| = 2, 3, 4, \dots$), the moving-frame distribution consists of periodic functions with two distinct frequencies, but because one is an integer multiple of the other, the power spectrum still consists of the fundamental frequency and its harmonics. More generally, $U(\eta', \tau')$ is time periodic if γ/ω is rational, and quasiperiodic otherwise. Unless $\gamma = \omega$ (the PGT), η' along characteristics will undergo a net (nonmonotonic) increase or decrease over each temporal period (Fig. 2), i.e., the distribution will propagate relative to the frame, and the transformed distribution will have temporal frequencies ω and $|\gamma|$.

As shown in the next subsection, our approach applies to a broad class of distributions having in common with the closed-form distribution (7) only the fact that they depend on two distinct periodic functions of linear combinations of position and time.

B. Theoretical underpinning

Let periodic functions $g_1(\zeta)$ and $g_2(\zeta)$ have periods T_1 and T_2 , respectively, so that $g_1(a_1\tau - b_1\eta)$ and $g_2(a_2\tau - b_2\eta)$ have temporal periods T_1/a_1 and T_2/a_2 , respectively, with corresponding temporal frequencies a_1/T_1 and a_2/T_2 . Thus, a spatiotemporal distribution q depending on η and τ through g_1 and g_2 according to

$$q(\eta, \tau) = S(g_1(a_1\tau - b_1\eta), g_2(a_2\tau - b_2\eta)) \quad (10)$$

will be temporally quasiperiodic if T_1/a_1 and T_2/a_2 are incommensurable. We note that q can be exact, or asymptotically represent long-time behavior following an initial transient.

Applying the Galilean transformation $\eta' = \eta - v\tau$, $\tau' = \tau$ to q gives the moving-frame distribution:

$$\begin{aligned} Q(\eta', \tau') &= q(\eta' + v\tau', \tau') \\ &= S(g_1[(a_1 - b_1v)\tau' - b_1\eta'], \\ &\quad g_2[(a_2 - b_2v)\tau' - b_2\eta']). \end{aligned} \quad (11)$$

Thus, a one-dimensional quasiperiodic distribution with spatiotemporal dependence only through two periodic functions [i.e., of the form (10)] will have two temporal frequencies varying with frame velocity as

$$f_1(v) = |\bar{a}_1 - \bar{b}_1v|, \quad (12a)$$

$$f_2(v) = |\bar{a}_2 - \bar{b}_2v|. \quad (12b)$$

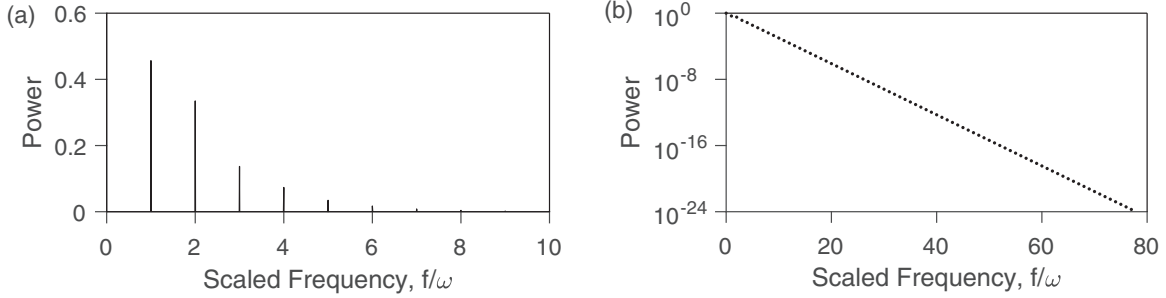


FIG. 4. Power spectrum (arbitrary units) of moving-frame time series $U(\eta'_{\text{PGT}} = 0.35, \tau')$ obtained from the quasiperiodic laboratory-frame distribution with incommensurable frequencies 1 and $\omega = \pi/5$, $\mu = 10$, and $u_0(\eta) = 1$, shown on (a) linear and (b) semilog bases. In (a), power levels of 1 and 9.95×10^{-4} at $f/\omega = 0$ and 10, respectively, are omitted for graphical clarity. In (b), asymptotic decay with frequency is exponential.

where $\bar{a}_i = a_i/T_i$ and $\bar{b}_i = b_i/T_i$ for $i = 1, 2$. The moving-frame distribution is time periodic if $f_1(v)$ and $f_2(v)$ are commensurable for a given v , so Q will be time periodic if there exists a pair of non-negative integers m and n with $m + n > 0$ such that

$$mf_1(v) = nf_2(v). \quad (13)$$

If $mn \neq 0$, we define $r = m/n$. For example, $r = 1$ corresponds to the case in which $g_1(a_1\tau - b_1\eta)$ and $g_2(a_2\tau - b_2\eta)$ have the same temporal frequency in the moving frame. The desired frame velocities for this case are $v = (\bar{a}_1 - \bar{a}_2)/(\bar{b}_1 - \bar{b}_2)$ and $v = (\bar{a}_1 + \bar{a}_2)/(\bar{b}_1 + \bar{b}_2)$, with only one being suitable in the singular case $|\bar{b}_1| = |\bar{b}_2|$.

Distributions can have multiple representations, e.g., $q(\eta, \tau) = 2 \sin(\tau + \eta) \sin(\pi\tau + 2\eta)$ is equivalent to $\cos((1-\pi)\tau - \eta) - \cos((1+\pi)\tau + 3\eta)$. In the first, $g_1(a_1\tau - b_1\eta) = \sin(\tau + \eta)$ and $g_2(a_2\tau - b_2\eta) = \sin(\pi\tau + 2\eta)$, so the frame-dependent frequencies are $f_1(v) = |1 + v|/(2\pi)$ and $f_2(v) = |\pi + 2v|/(2\pi)$, and $v = 1 - \pi$ and $v = -(1 + \pi)/3$ give moving-frame periodicity with $r = 1$. Using the second representation gives $f_1(v) = |1 - \pi - v|/(2\pi)$ and $f_2(v) = |1 + \pi + 3v|/(2\pi)$, with $v = -\pi/2$ and $v = -1$ for $r = 1$. As both representations describe the same distribution, a velocity satisfying (13) for these or other representations renders the distribution time periodic in the associated moving frame. For different representations, one can generate the same frame velocities by solving (13) using different (m, n) combinations. Other sets of velocities can thus be identified by varying r or allowing $mn = 0$, or by using other representations with the same (m, n) .

Consistent with the lack of an analytical representation in experimental and observational data, no explicit representation of the distribution is needed. The distribution need only have the properties associated with (10), from which it follows that fixed-location time series will have power spectra whose observed frequencies are linear combinations of two incommensurable frequencies. As for all quasiperiodic time series, the choice of these incommensurable frequencies is not unique. Furthermore, in any Galilean frame with velocity v , the moving-frame distribution Q (11) will be quasiperiodic with observed frequencies that are linear combinations of two incommensurable frequencies, unless the Galilean transformation renders the distribution time periodic. We refer to

any pair of incommensurable frequencies obtainable from the observed frequencies in the power spectrum for a given frame velocity as “basis frequencies” and refer to a particular pair determined from the observed frequencies as “extracted frequencies,” $f_{E,A}$ and $f_{E,B}$. For distributions time periodic in a given moving frame, the pair of extracted frequencies, and any other pair of basis frequencies, will consist of one positive frequency and either a second positive frequency rationally related to it, or a zero “frequency.” This approach allows for continuous dependence of basis frequencies on frame velocity, as discussed below.

At any frame velocity, each member of each pair of basis frequencies lies on a piecewise-linear continuous function of frame velocity [(12a), (12b)]. In other words, at a given frame velocity, the values of these piecewise-linear functions correspond to a pair of basis frequencies for that moving frame. We refer to such piecewise-linear functions as “frequency lines,” $f_1(v)$ and $f_2(v)$. Note that frequency lines must be paired such that at each moving-frame velocity, they correspond to a pair of basis frequencies. Correct pairing of frequency lines can be confirmed if, at some frame velocity, the pair coincides with a pair of incommensurable basis frequencies. If frequency-line pairs of the form (12a), (12b) exist, then the moving-frame distribution Q is time periodic in frames for which the corresponding pair of frequencies is rationally related, i.e., satisfy (13). If such frequency-line pairs do not exist, then q is not of the form (10). Since there is a countably infinite number of pairs of basis frequencies for any given v , there will also be a countably infinite number of frequency-line pairs, any of which can be used to satisfy (13). An example application of this approach is given in Sec. III D. Generalization to two or three dimensions and to distributions with more than two basis frequencies is discussed in Sec. IV.

C. Procedure to determine frame velocity for one-dimensional experimental data

To illustrate application of our approach in the context of experimental data, we consider discrete-time time series at discrete locations provided from a temporally quasiperiodic one-dimensional distribution $q(\eta, \tau)$, without knowing the functional form of the distribution itself. At each location, one can use the laboratory-frame time series to determine the power spectrum, consisting of a set of discrete observed

frequencies, each representable as a linear combination of the same pair of incommensurable basis frequencies, the choice of which is not unique.

We consider four cases based on different spatial and temporal resolutions relative to spatial and temporal variation of the data, corresponding to whether accurate interpolation in space or time is possible. In each case, we assume that the data are acquired over a domain $\eta_{\min} \leq \eta \leq \eta_{\max}$ and a time period $\tau_1 \leq \tau \leq \tau_{\max}$, with uniform spacing $\Delta\eta$ and uniform temporal increment $\Delta\tau$, respectively. (If the spatial or temporal resolution is sufficient to accurately interpolate, increments need not be uniform.) We also assume that quasiperiodic behavior has been established by τ_1 , possibly following an initial transient. Because the power spectrum is in the frequency domain, $\tau_{\max} - \tau_1$ should be large enough for the Fourier transform to provide adequate frequency resolution. As discussed below, a large $\eta_{\max} - \eta_{\min}$ is preferred, especially when sufficiently accurate spatial interpolation is not possible, in order to have a large range of possible frame velocities. In each of the four cases, we construct (with minor variations depending on resolution) discrete-time moving-frame time series analogous to the continuous moving-frame time series obtained from the distribution $U(\eta'_{\text{PGT}}, \tau')$ discussed in Sec. III A and determine extracted frequencies in the moving frames, from which we calculate frequency-line pairs.

In each of the four cases below, applicability of the approach is not restricted to temporally quasiperiodic distributions corresponding to sums of periodic functions of their arguments. This is made clear by reference to (7), which has a highly nonlinear dependence of $u(\eta, \tau)$ on trigonometric functions, and more generally by (10).

1. High resolution in time and space

Data at each location are often sampled at a sufficiently high rate to allow accurate interpolation in time. For such data acquired either on a continuous basis (e.g., with a streak camera [44]) or discretely (e.g., with a camera having finite “shutter speed”), spatial resolution will typically be very high, allowing for spatial interpolation as necessary. This is also usually the case for numerical simulations. Here, we deal with these cases as if the data are or can be treated as continuous in space and time.

We process the data to mimic an observer moving through the distribution with constant nonzero velocity v , as illustrated in Fig. 5. We construct I moving-frame time series by sampling data along the lines $\eta - \eta_i = v(\tau - \tau_1)$, beginning at $\tau = \tau_1$ for I arbitrarily chosen positions η_i (not necessarily at measurement locations) in $\eta_{\min} \leq \eta_i \leq \eta_{\max}$. Here, either the spatial increment $\Delta\eta_{\text{mf}}$ (lab-frame distance between consecutive points in each moving-frame time series; see Fig. 5) or temporal increment $\Delta\tau_{\text{mf}} = \Delta\eta_{\text{mf}}/v$ is arbitrarily chosen, with $\text{sgn}(\Delta\eta_{\text{mf}}) = \text{sgn}(v)$. The i th moving-frame time series is then

$$Q_{v,i}(\tau'_1 + j\Delta\tau') = q(\eta_i + j\Delta\eta_{\text{mf}}, \tau_1 + j\Delta\tau_{\text{mf}}), \quad (14)$$

for $1 \leq i \leq I$ and $0 \leq j \leq \min\{(\tau_{\max} - \tau_1)/\Delta\tau_{\text{mf}}, \max[(\eta_{\min} - \eta_i)/\Delta\eta_{\text{mf}}, (\eta_{\max} - \eta_i)/\Delta\eta_{\text{mf}}]\}$, where $\tau'_1 = \tau_1$ and $\Delta\tau' = \Delta\tau_{\text{mf}}$. The upper bound on j accounts for the decrease in the number of elements in the i th time series as

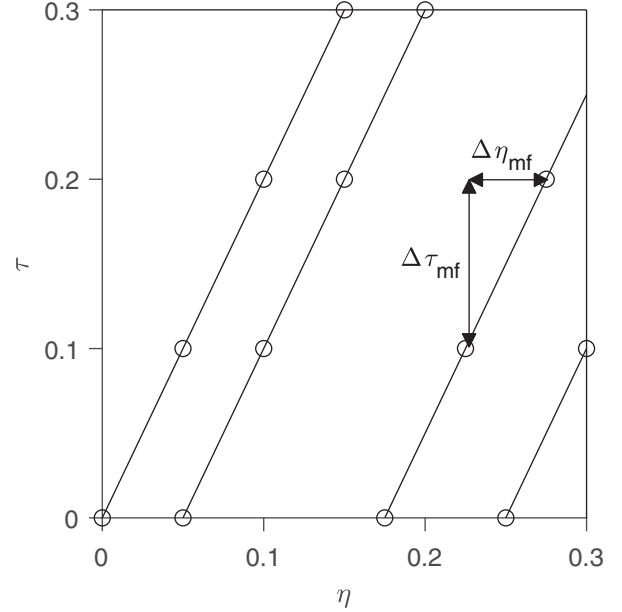


FIG. 5. Four moving-frame time series constructed from laboratory-frame data. Each consists of discrete points along a line whose slope is the reciprocal of frame velocity ($v = 0.5$ here). Data are sampled with a time increment of $\Delta\tau_{\text{mf}} = \Delta\eta_{\text{mf}}/v = 0.1$. Intersections of the moving-frame time series with the $\tau = 0$ axis are at $\eta_1 = 0$, $\eta_2 = 0.05$, $\eta_3 = 0.175$, and $\eta_4 = 0.25$), with no requirement that $\eta_i - \eta_{i-1}$ be uniform. For $v > 0$, moving-frame time series with larger η_i have fewer points than those with smaller η_i .

η_i approaches the domain boundary toward which the line in the η - τ plane moves. Larger v values give moving-frame time series with shorter duration because the line in the η - τ plane reaches the domain boundary earlier, so v and η_i should be chosen to maximize the duration of time series (which maximizes frequency resolution of power spectra).

Basis frequencies depend only on frame velocity and not on choice of time series (i.e., η_i) within that frame, so in principle $I = 1$ is sufficient. However, inadequate spatial or temporal resolution can require interpolation and thus introduce interpolation error, and the spatial extent and temporal duration of any particular dataset will limit the duration of the moving-frame time series, which limits the frequency resolution of the Fourier transform. These errors and resolution limitations can be mitigated by examining additional time series for each frame velocity, each of which will have observed frequencies that can be generated from the same basis frequencies.

For each time series and for several values of v , we generate the power spectrum and determine a pair of extracted frequencies, $f_{E,A}$ and $f_{E,B}$, from which we calculate several pairs of basis frequencies, e.g., $f_{E,A}$ and $f_{E,A} + f_{E,B}$. (If $f_{E,A}$ and $f_{E,B}$ are extracted frequencies, then $f_{E,A}$ and $|pf_{E,A} + f_{E,B}|$ also constitute a pair of basis frequencies for any integer p , as do $f_{E,B}$ and $|f_{E,A} + pf_{E,B}|$. Other choices are also possible.) We then identify a frequency-line pair $f_1(v)$ and $f_2(v)$ for which pairs of basis frequencies depend on the absolute values of linear functions of v , i.e., of the form (12a), (12b). Since for each value of v it is not known *a priori* which

basis frequencies correspond to which frequency lines, several values of v might be needed to make the pattern apparent. Sufficient conditions for $f_1(v)$ and $f_2(v)$ to be a frequency-line pair are that they are of the form (12a), (12b), that they pass through a pair of basis frequencies for each v considered, and that there is at least one v for which those frequencies are incommensurable. Once the continuous, piecewise-linear functions $f_1(v)$ and $f_2(v)$ have been determined, different rational r (and combinations of m and n such that $mn \neq 0$) can be used in (13) to find frame velocities v such that Galilean transformation will render the moving-frame distribution time periodic.

This procedure is demonstrated in Sec. III D for spatially- and temporally-discretized data generated from the example distribution (7).

2. High resolution in time, low resolution in space

This case is of interest in two distinct classes of situations. In the first, data are taken with sensors (e.g., hot-wire anemometers, electrodes, pyrometers and other thermal sensors) far enough apart that spatial interpolation is problematic. In the second class, which includes several magnetic resonance velocimetry techniques, spatial resolution is low for any instantaneous measurement, and can be improved by temporally aggregating data sampled over long time periods [14] or at high rates [45]. Such velocimetry techniques are well suited to steady and time-periodic flows, but can be applied to temporally more complex flows with trade-offs between spatial and temporal resolution [46].

The data are typically available on a uniformly-spaced grid, so the following approach or its two- and three-dimensional generalizations (see Sec. IV) can be followed. If the temporal sampling rate is sufficiently high, one can freely choose v and choose $\Delta\eta_{mf} = \pm\Delta\eta$, with $\text{sgn}(\Delta\eta_{mf}) = \text{sgn}(v)$, as the signed distance between sensor locations, with $\eta_i = \eta_{\min} + (i-1)|\Delta\eta_{mf}|$. This will determine $\Delta\tau_{mf} = \Delta\eta_{mf}/v$, and ensure that each spatial location $\eta_i + j\Delta\eta_{mf}$ sampled coincides with a sensor location, so that spatial interpolation is unnecessary. The moving-frame time series are then constructed as above using (14), requiring only a subset of the I time series.

Once the moving-frame time series are constructed, we proceed as in the case of essentially continuous temporal and spatial data. If the number of measurement locations is small, the number of elements in the moving-frame time series will be limited to no more than the number of measurement locations, with a consequent reduction in the accuracy with which frequency can be determined. A trade-off exists between large-magnitude v with moving-frame time series having many elements, and small-magnitude v with time series having greater temporal extent.

3. Low resolution in time, high resolution in space

This case is very similar to the case of high temporal resolution and low spatial resolution. Assuming that the data are sampled with constant time-step size $\Delta\tau$, we can choose v and η_i arbitrarily and determine $\Delta\eta_{mf}$ from $\Delta\tau_{mf} = \Delta\tau$ and $\Delta\eta_{mf} = v\Delta\tau_{mf}$, and then construct the time series using (14). We proceed exactly as in the case of essentially continuous temporal and spatial data, with the limitation that the number

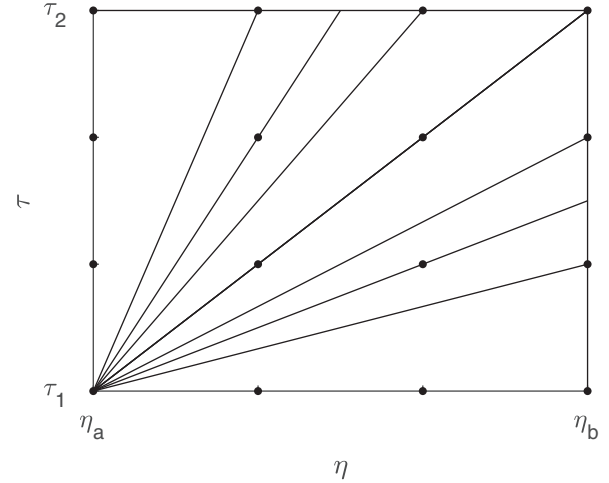


FIG. 6. Moving frames that can be chosen beginning at a particular spatiotemporal point for a dataset with low spatial and temporal resolution. Frames indicated are nontrivial in the sense that each passes through at least one point for $\tau > \tau_1$ and has nonzero velocity.

of elements in the time series cannot exceed the number of measurement times, thus limiting the accuracy with which frequency can be determined.

4. Low resolution in time and space

In this case, the resolution is insufficient to support temporal or spatial interpolation, such as for concentration measurements in rivers [47]. (This is sometimes the case in three-dimensional imaging, e.g., particle image velocimetry [11] or “4D” computed tomography [48], where trade-offs are made between temporal and spatial resolution when scanning is performed in a third dimension. These cases can be treated with the two- and three-dimensional generalizations of the procedure below, as discussed in Sec. IV.) Thus, values of v are no longer chosen at will, but rather from a finite set defined by $v = l_1\Delta\eta/(l_2\Delta\tau)$, where l_1 is a nonzero integer whose magnitude is less than the number of measurement locations and l_2 is a positive integer no larger than the number of time steps, assuming that measurements are uniformly distributed over $\eta_{\min} \leq \eta \leq \eta_{\max}$ with spacing $\Delta\eta$ and that data are sampled over $\tau_1 \leq \tau \leq \tau_{\max}$ at a constant rate $1/\Delta\tau$. Here, $\Delta\eta_{mf} = l_1\Delta\eta$ and $\Delta\tau_{mf} = l_2\Delta\tau$ for integer l_1 and l_2 . Figure 6 illustrates possible choices of v . After v is chosen, the I moving-frame time series are constructed as above using (14), with $\eta_i + j\Delta\eta_{mf} = \eta_{\min} + (i + jl_1 - 1)\Delta\eta$, though only a subset of them need be used.

After the time series are constructed, the analysis again proceeds as with essentially continuous temporal and spatial data. The limitation noted for high temporal resolution and low spatial resolution applies here, with the number of elements in the moving-frame time series not exceeding the smaller of the number of measurement locations and the number of measurement times, thus limiting the accuracy with which frequency can be determined.

D. Example application of procedure to numerical data

To illustrate use of this procedure, a discretized spatiotemporal dataset was created from the example distribution (7) with $u_0(\eta) = 1$, $\mu = 10$, and $\omega = \pi/5$, over the ranges $-10^4 \leq \eta \leq 2 \times 10^4$ and $0 \leq \tau \leq 10^5$, sampled with increments $\Delta\eta = 10^{-3}$ and $\Delta\tau = 10^{-4}$. Here, we demonstrate application of our procedure without using knowledge of the functional form used to create the data. To clearly demonstrate that our approach transforms a quasiperiodic distribution to one that is time periodic in a moving frame, with power spectra consisting of a single frequency and its harmonics, we compute frequencies to five significant digits for a wide range of frame velocities, which requires a number of times (10^9) and number of spatial locations (3×10^7) not typical of experimental data. Two or three significant digits in the frequencies, more common in experimental work, are achievable with realistic numbers of temporal and spatial points, and construction and analysis of multiple time series for a given frame velocity can mitigate error attributable either to interpolation or to use of time series with limited duration and resolution.

For frame velocities $v = -0.10, -0.08, -0.06, \dots, 0.18, 0.20$, we construct moving-frame time series originating at $(\eta', \tau') = (0, 0)$ with temporal increment $\Delta\tau_{mf} = 5 \times 10^{-3}$. (The same analysis could have been applied to data with smaller spatial extent by either varying η_i or by using smaller values of v , both of which can be chosen arbitrarily subject to adequate spatial and temporal interpolation.) Because interpolation errors are small and each time series covers a large temporal range, we examine only a single time series in each frame. For each v , we Fourier transform the time series and identify N_o observed frequencies. Here, we arbitrarily take these frequencies to be those with $f \leq 10$ having peaks in the power spectrum with at least one one-thousandth the power of the most energetic peak. (See Supplemental Material Sec. C [43] for supporting plots and table for four representative frame velocities. For those velocities, $N_o = 26, 16, 4$, and 25.) For each frame velocity, the observed frequencies can be formed by summing integer multiples of at most two incommensurable frequencies, so that for each frame we determine a pair of extracted frequencies $f_{E,A}$ and $f_{E,B}$, using zero as the second extracted frequency when the moving-frame distribution is observed to be time periodic.

As explained above, a pair of extracted frequencies, or one extracted frequency and either the sum or difference of the pair, constitute a pair of basis frequencies. The four frequencies $f_{E,A}$, $f_{E,B}$, $f_{E,A} + f_{E,B}$, and $|f_{E,A} - f_{E,B}|$ are plotted in Fig. 7 for each frame velocity. While it is possible that all pairs of extracted frequencies lie on the same two frequency lines, this is extremely unlikely, so several other basis pairs are plotted to aid in identifying frequency lines. We designate for subsequent use “primary frequency lines” $f_1(v) = 0.62832$ and $f_2(v) = |1 - 10v|$ (shown as solid lines in Fig. 7) which have the desired form (12a), (12b) and pass through a pair of basis frequencies at each v considered. (Although in Fig. 7 we restricted the frequencies plotted to the four above, at $v = 0.08$ the basis frequency pair $f_{E,A} + 3f_{E,B}$ and $f_{E,B}$, with $f_{E,A} = 0.02832$ and $f_{E,B} = 0.20000$, lies on the primary frequency lines $f_1(v)$ and $f_2(v)$, respectively.) We note that $f_1(v)$ is a five-digit approximation to $\pi/5$, and that for

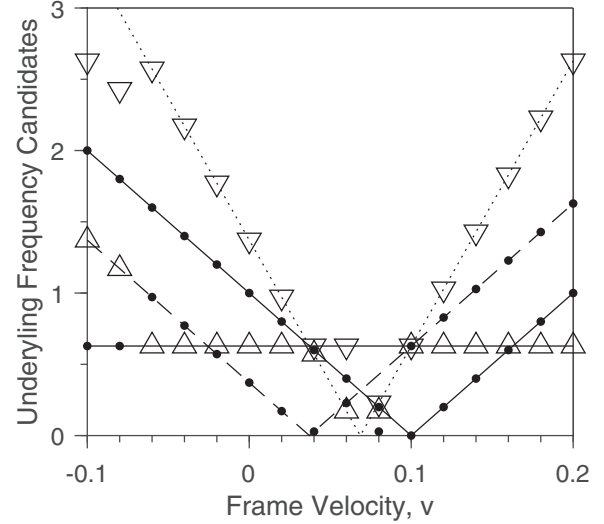


FIG. 7. Extracted frequencies, their sum, and the absolute value of their difference (\bullet : $f_{E,A}$ and $f_{E,B}$; ∇ : $f_{E,A} + f_{E,B}$; Δ : $|f_{E,A} - f_{E,B}|$) for 16 frame velocities. The “primary frequency lines,” i.e., basis frequencies vs frame velocity, are shown as solid lines (equations given in text), and two additional frequency lines are shown as a dotted line and as a dashed line (“paired equations” given in text). The two parts of each frequency line have slopes of equal magnitude. The absence of a marker on the $f_1(v)$ primary frequency line at $v = 0.08$ is due to our choice to plot only the four frequencies above. At $v = 0.08$, the basis frequency pair $f_{E,A} + 3f_{E,B}$ and $f_{E,B}$, with $f_{E,A} = 0.02832$ and $f_{E,B} = 0.20000$, lies on the primary frequency lines $f_1(v)$ and $f_2(v)$, respectively.

any computation with finite-precision arithmetic, the observed frequencies (and hence the extracted frequencies and other basis frequencies) will be rational. In this context, we say that two frequencies are incommensurable if they are not equal to the ratio of two “small” integers, i.e., with magnitudes much smaller than the reciprocal of the frequency discretization of the Fourier transform.

For any rational r (and for non-negative integers m and n with $m + n > mn = 0$), v satisfying (13) gives a reference frame in which the distribution is time periodic. Examples are $v = (1 - 0.62832)/10$ and $v = (1 + 0.62832)/10$ for $r = 1$, with the corresponding spatiotemporal distributions in these frames plotted in Figs. 8(a) and 8(c). Figures 8(b) and 8(d) show that the power spectra of the $U(\eta' = 0, \tau')$ time series in these two frames consist of a fundamental frequency and its harmonics, confirming that the approach has indeed identified frames in which the distribution is time periodic. Figures 3 and 8(a) are indistinguishable, as expected, showing that the numerical procedure can arrive at the same Galilean transformations as did the analytical approach for the closed-form distribution in Sec. III A. Additional frame velocities can be obtained by choosing other pairs of m and n , such as $v = 0.1$ for $n > m = 0$. For every combination of $n \neq 0$ and m in (13), the frame velocities $v = (1 \pm 0.62832 m/n)/10$, which are finite-precision equivalents of the condition derived in Sec. III A, will render the distribution time periodic.

Figure 7 also shows that the paired equations $f_1(v) = |2(1 - 10v) - 0.62832|$ and $f_2(v) = |1 - 10v|$,

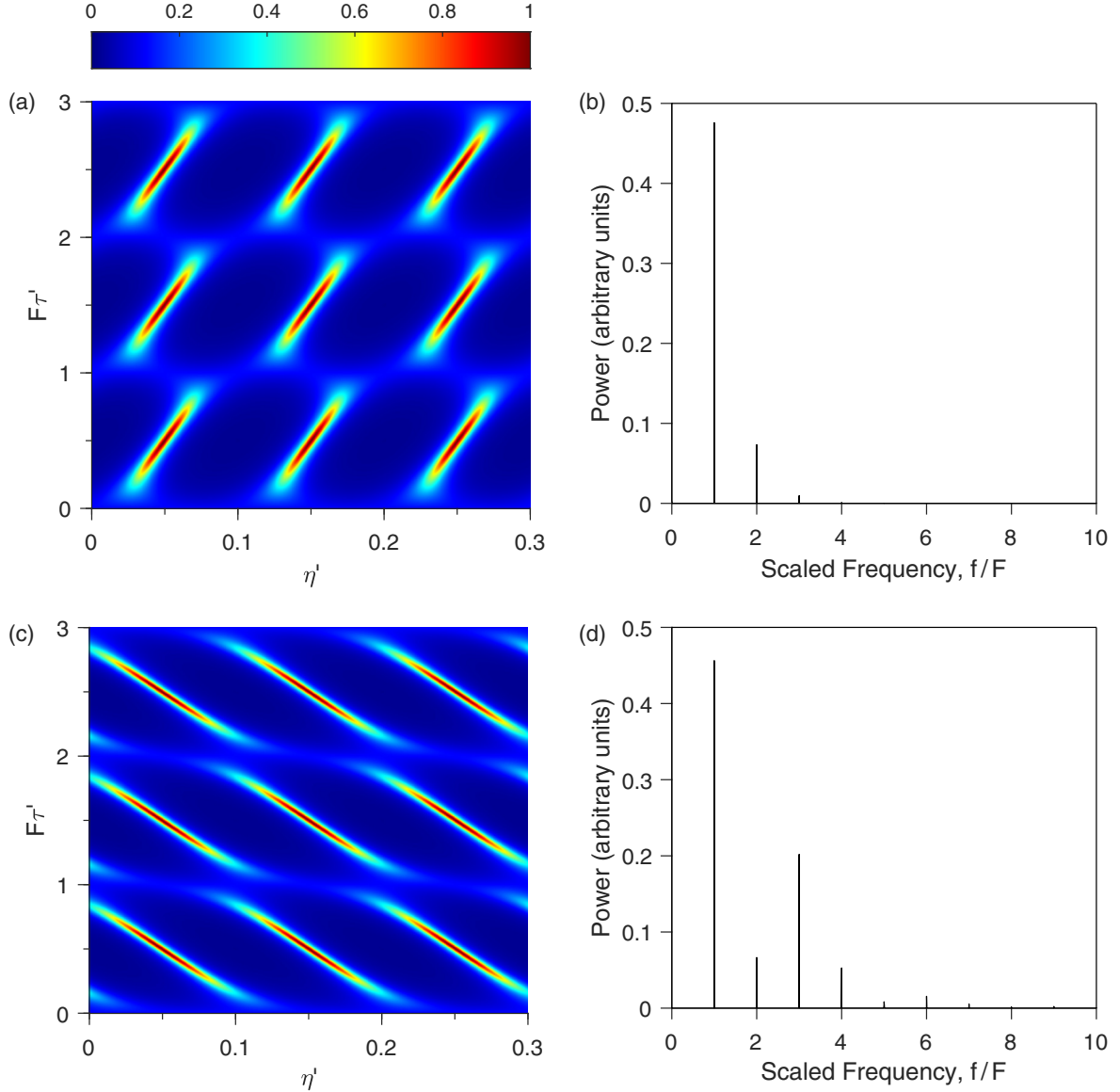


FIG. 8. Variation of $U(\eta', \tau')$, with the intrinsic frequency $\omega = \pi/5$ (incommensurable with the extrinsic frequency 1), $\mu = 10$, and $u_0(\eta) = 1$, in the moving frames with (a) $v = (1 - 0.62832)/10$ and (c) $v = (1 + 0.62832)/10$, with magnitude scaled by $8.007 = \max[U(\eta', \tau')]$. These frame velocities were determined as intersections of the frequency-line pair $f_1(v) = 0.62832$ and $f_2(v) = |1 - 10v|$, i.e., by solving (13) with $r = m/n = 1$. As expected, the distribution is time periodic in both frames, as shown by the power spectra of the $U(\eta' = 0, \tau')$ time series for (b) $v = (1 - 0.62832)/10$ and (d) $v = (1 + 0.62832)/10$. In (b) and (d), the peak at $f = 0$ is omitted for graphical clarity. The symbol F denotes the value 0.62832 in each subfigure.

$f_1(v) = |(1 - 10v) - 0.62832|$ and $f_2(v) = |1 - 10v|$, $f_1(v) = 0.62832$ and $f_2(v) = |(1 - 10v) - 0.62832|$, and $f_1(v) = |2(1 - 10v) - 0.62832|$ and $f_2(v) = |1 - 10v|$ describe valid choices of frequency-line pairs. As discussed in Sec. III B, there is a countably infinite set of frequency-line pairs, such as $f_1(v) = |p(1 - 10v) - 0.62832|$ and $f_2(v) = |1 - 10v|$ for integer p , and each pair could be used, by solving (13) for different (m, n) combinations, to identify frames in which the distribution is rendered time periodic. Within the accuracy of finite-precision arithmetic, the set of frame velocities rendering the distribution time periodic is independent of the choice of frequency-line pair.

IV. MULTIDIMENSIONAL GENERALIZATION

The approach can be extended to more complex situations. We consider a distribution $q(\boldsymbol{\eta}, \tau)$, quasiperiodic in time τ , whose spatiotemporal variation can be represented in terms of $2 \leq N_f < \infty$ periodic functions g_i , each having a single argument of the form

$$\zeta_i = a_i \tau - \mathbf{b}_i \cdot \boldsymbol{\eta}, \quad 1 \leq i \leq N_f, \quad (15)$$

where $\boldsymbol{\eta}$ is an N_d -dimensional position vector and for $1 \leq i \leq N_f$, g_i has period T_i , \mathbf{b}_i is an N_d -dimensional vector, and, without loss of generality, $a_i \geq 0$. In other words, q is of the

form

$$q(\boldsymbol{\eta}, \tau) = R(g_1(a_1\tau - \mathbf{b}_1 \cdot \boldsymbol{\eta}), g_2(a_2\tau - \mathbf{b}_2 \cdot \boldsymbol{\eta}), \dots, g_{N_f}(a_{N_f}\tau - \mathbf{b}_{N_f} \cdot \boldsymbol{\eta})). \quad (16)$$

For Cartesian $\boldsymbol{\eta}$, a Galilean transformation $\boldsymbol{\eta}' = \boldsymbol{\eta} - \mathbf{v}\tau$, $\tau' = \tau$ renders $Q(\boldsymbol{\eta}', \tau') = q(\boldsymbol{\eta}' + \mathbf{v}\tau', \tau') = q(\boldsymbol{\eta}, \tau)$ time periodic in a moving frame if there exist ψ , \mathbf{v} , and rational r_i ($1 \leq i \leq N_f$) such that

$$|\bar{a}_i - \bar{\mathbf{b}}_i \cdot \mathbf{v}| = r_i\psi, \quad 1 \leq i \leq N_f, \quad (17)$$

where $\bar{a}_i = a_i/T_i$ and $\bar{\mathbf{b}}_i = \mathbf{b}_i/T_i$ for $1 \leq i \leq N_f$.

Some distributions with spatial variation more complex than allowed by (16) can be treated similarly, as discussed in Supplemental Material Sec. D [43].

For $N_f > 2$, there are combinations of \bar{a}_i and $\bar{\mathbf{b}}_i$ such that (17) does not admit a solution $(\mathbf{v}, \psi, \mathbf{r})$ with the N_f elements of \mathbf{r} rational. A simple example for $N_d = 1$ and $N_f = 3$ is $\bar{a}_1 = \bar{a}_2 = \bar{a}_3 = 1$, $\bar{b}_1 = 0$, $\bar{b}_2 = 1$, and $\bar{b}_3 = \pi$. On the other hand, it can be shown that a solution exists for $N_d = 1$ and $N_f = 3$ if $(\bar{a}_i\bar{b}_j - \bar{a}_j\bar{b}_i)/(\bar{a}_k\bar{b}_j - \bar{a}_j\bar{b}_k)$ is rational, where (i, j, k) is some cyclic permutation of (1,2,3). In general, valid solutions will exist if $N_d + 1 \geq N_f$ or if $N_f - N_d - 1$ conditions on \bar{a}_i and \bar{b}_i , such as shown above, are satisfied, except in degenerate cases, as discussed in Supplemental Material Sec. E [43].

The approach for determining appropriate frame velocities from experimental data, described in Secs. III B and III C and illustrated in Sec. III D for one Cartesian dimension ($N_d = 1$) with $N_f = 2$, can be extended to two- and three-dimensional data (i.e., $N_d = 2, 3$) with more complicated spatiotemporal structure (i.e., $N_f > 2$). As per the discussion in Sec. III B, the distribution need only have the properties associated with (16), with no analytical representation required. If adequate moving-frame time series can be constructed from the laboratory-frame data, the N_o observed frequencies for each moving frame will consist of linear combinations of no more than N_f incommensurable frequencies, with degeneracy sometimes leading to fewer when some of the N_f basis frequencies are zero or rationally related. After calculating sets of these basis frequencies (whose accuracy will depend on the temporal duration of, and the number of elements in, the moving-frame time series, as well as on interpolation error) for a sufficient number of moving frames, one can calculate sets of N_f objects

$$f_i(\mathbf{v}) = |\bar{a}_i - \bar{\mathbf{b}}_i \cdot \mathbf{v}|, \quad 1 \leq i \leq N_f \quad (18)$$

that are N_d -dimensional generalizations of the $N_d = 1$ frequency lines (two nonparallel rays with a common end point and equal-magnitude slopes). For $N_d = 2$, each object consists of two nonparallel half planes in \mathbb{R}^3 with a common edge. For $N_d = 3$, the objects consist of piecewise hyperplanes in \mathbb{R}^4 . (Further characterization is provided in Supplemental Material Sec. F [43], which includes Ref. [49].) As with the need to pair frequency lines in the $N_d = 1$ case, these objects must be grouped into sets such that they constitute a set of N_f basis frequencies for any frame velocity \mathbf{v} . That the objects have been correctly grouped into a set can be confirmed if there exists a \mathbf{v} for which these basis frequencies are pairwise incommensurable. If construction of such a set is not possible,

then the distribution is not of the form (16). If at a given frame velocity \mathbf{v} , each of the N_f objects corresponds to a frequency rationally related to all the others or equal to zero, then the frame velocity \mathbf{v} will render the distribution periodic. For each of the countably infinite number of such sets of objects, the lab-frame distribution q will be rendered time periodic in any frame with velocity \mathbf{v} satisfying (17), as discussed in Secs. III B–D.

The techniques described above can be applied to some distributions exhibiting temporally quasiperiodic behavior and nonrectilinear propagation, if the spatiotemporal variation satisfies (16), or (S6) and (S7) in the Supplemental Material Sec. D [43], with $\boldsymbol{\eta}$ no longer required to be Cartesian. For example, these techniques can be applied to helical propagation [50–56] if the arguments of the periodic functions are of the form $a_m\tau - b_mz - c_m\phi$, where z and ϕ are the axial and azimuthal coordinates, respectively, in a circular cylindrical system. The approach is also applicable when various helical coordinate systems [57,58] are used and, in fact, can be applied to any distribution having the properties associated with the form (16) regardless of coordinate system.

V. DISCUSSION AND CONCLUSIONS

We note that in systems with diffusion, heat conduction, viscosity, or other dissipative effects, temporally periodic or quasiperiodic long-time behavior typically follows an initial transient, and depends on internal or boundary forcing or on nonlinearity. Our approach is clearly applicable to long-time quasiperiodic behavior preceded by a transient of different type.

The approach described can be applied in the presence of noise. The Galilean transformation applies independently to the distribution $q(\boldsymbol{\eta}, \tau)$ and a noise process $w(\boldsymbol{\eta}, \tau)$, leaving the relationship between signal and noise effectively unchanged. Thus, a distribution with additive noise transforms from $q(\boldsymbol{\eta}, \tau) + w(\boldsymbol{\eta}, \tau)$ to $Q(\boldsymbol{\eta}', \tau') + W(\boldsymbol{\eta}', \tau')$, and a distribution with multiplicative noise transforms from $q(\boldsymbol{\eta}, \tau)[1 + w(\boldsymbol{\eta}, \tau)]$ to $Q(\boldsymbol{\eta}', \tau')[1 + W(\boldsymbol{\eta}', \tau')]$. Extraction of basis frequencies from power spectra of time series will be unaffected by noise provided that its amplitude is sufficiently low. Similarly, extraction of basis frequencies will be unaffected if the power spectrum of the noise process does not significantly overlap with the power spectrum of the distribution being examined. For somewhat higher noise amplitudes, statistical stationarity, statistical homogeneity, and lack of spatiotemporal correlation of the noise become important in determining whether the distribution's moving-frame frequency content can be identified.

Because Galilean transformation has no effect on additional independent variables (i.e., those other than position and time), our transformation will also be applicable to situations in which the propagating spatiotemporal quantity is a distribution function depending unrestrictedly on, for example, particle, drop, or bubble size, particle or molecular orientation, or particle momentum. An example of the latter is provided by a modified Fokker-Planck analysis of the distribution of particles, depending on position, time, and momentum, in a temporally quasiperiodic flow [59].

We also note that transformation of a propagating distribution $q(\eta, \tau)$ temporally quasiperiodic at each point η in the laboratory frame to a distribution $Q(\eta', \tau')$ time periodic at each point η' in the moving frame is equivalent to reducing the correlation dimension [60] of the time series. Thus, in the most common case of two incommensurable temporal frequencies in the laboratory-frame distribution, corresponding to the time series of q at each spatial point η having correlation dimension two, the time series of Q at each point η' in the moving frame will have correlation dimension one.

In conclusion, a broad class of propagating distributions in one, two, or three spatial dimensions, with temporal behavior

quasiperiodic in a laboratory frame, can be rendered time periodic in a moving frame by Galilean transformation. Sufficient conditions for this to work, and the resulting transformations, are discussed, and a process is established to identify such transformations for spatially- and temporally-discretized experimental data.

ACKNOWLEDGMENTS

This work was supported by DOE Grant No. DE-EE0007888, and by NSF Grant No. 16-24812 through the Center for Advanced Research in Drying. The support of Siemens PLM is also gratefully acknowledged.

- [1] *Measurements in Heat Transfer*, 2nd ed., edited by E. R. G. Eckert and R. J. Goldstein (Hemisphere Publishing, London, 1977).
- [2] T. E. Langford, The temperature of a British river upstream and downstream of a heated discharge from a power station, *Hydrobiologia* **35**, 353 (1970).
- [3] P. Van Shaw, L. P. Reiss, and T. J. Hanratty, Rates of turbulent transfer to a pipe wall in the mass transfer entry region, *AIChE J.* **9**, 362 (1963).
- [4] R. J. Goldstein, *Fluid Mechanics Measurements* (Taylor & Francis, Washington, 1996), 2nd ed.
- [5] F. Durst, A. Melling, and J. H. Whitelaw, *Principles and Practice of Laser-Doppler Anemometry*, 2nd ed. (Academic Press, New York, 1981).
- [6] J. E. Mitchell and T. J. Hanratty, A study of turbulence at a wall using an electrochemical wall shear-stress meter, *J. Fluid Mech.* **26**, 199 (1966).
- [7] L. L. Beranek, *Acoustical Measurements* (Acoustical Society of America, New York, 1988).
- [8] B. E. Thompson and J. H. Whitelaw, Flying hot-wire anemometry, *Exp. Fluids* **2**, 47 (1984).
- [9] H. S. Rhee, J. R. Koseff, and R. L. Street, Flow visualization of a recirculating flow by rheoscopic liquid and liquid crystal techniques, *Exp. Fluids* **2**, 57 (1984).
- [10] J. Sakakibara and R. J. Adrian, Whole field measurement of temperature in water using two-color laser induced fluorescence, *Exp. Fluids* **26**, 7 (1999).
- [11] R. J. Adrian and J. Westerweel, *Particle Image Velocimetry* (Cambridge University Press, Cambridge, 2011).
- [12] R. K. Hanson, Planar laser-induced fluorescence imaging, *J. Quant. Spectrosc. Radiat. Transfer* **40**, 343 (1988).
- [13] J. E. Dove and H. G. Wagner, in *Eighth Symposium (International) on Combustion, Pasadena, 1960* (Williams & Wilkins Co., Baltimore, 1962), p. 589.
- [14] D. N. Ku, C. L. Biancheri, R. I. Pettigrew, J. W. Peifer, C. P. Markou, and H. Engels, Evaluation of magnetic resonance velocimetry for steady flow, *ASME J. Bio. Mech. Eng.* **112**, 464 (1990).
- [15] R. Miles, C. Cohen, J. Connors, P. Howard, S. Huang, E. Markovitz, and G. Russell, Velocity measurements by vibrational tagging and fluorescent probing of oxygen, *Opt. Lett.* **12**, 861 (1987).
- [16] H. Hu, Z. Jin, D. Nocera, C. Lum, and M. Koochesfahani, Experimental investigations of micro-scale flow and heat transfer phenomena by using molecular tagging techniques, *Meas. Sci. Technol.* **21**, 085401 (2010).
- [17] Q. Ouyang, V. Castets, J. Boissanade, J. C. Roux, P. De Kepper, and H. L. Swinney, Sustained patterns in chlorite-iodide reactions in a one-dimensional reactor, *J. Chem. Phys.* **95**, 351 (1991).
- [18] A. Tóth, V. Gáspár, and K. Showalter, Signal transmission in chemical systems: Propagation of chemical waves through capillary tubes, *J. Phys. Chem.* **98**, 522 (1994).
- [19] N. Manz, S. C. Müller, and O. Steinbock, Anomalous dispersion of chemical waves in a homogeneously catalyzed reaction system, *J. Phys. Chem. A* **104**, 5895 (2000).
- [20] K. Miyakawa, T. Okano, and T. Tanaka, Noise-induced spatiotemporal dynamics in a linear array of excitable chemical oscillators, *Phys. Rev. E* **71**, 066202 (2005).
- [21] J. Miyazaki and S. Kinoshita, Stopping and initiation of a chemical pulse at the interface of excitable media with different diffusivity, *Phys. Rev. E* **76**, 066201 (2007).
- [22] D. G. Míguez, P. McGraw, A. P. Muñozuri, and M. Menzinger, Selection of flow-distributed oscillation and Turing patterns by boundary forcing in a linearly growing, oscillating medium, *Phys. Rev. E* **80**, 026208 (2009).
- [23] M. Markus and K. Stavridis, Observation of chemical turbulence in the Belousov-Zhabotinsky reaction, *Int. J. Bifurc. Chaos* **4**, 1233 (1994).
- [24] S. B. Margolis, The asymptotic theory of gasless combustion synthesis, *Metall. Trans. A* **23A**, 15 (1992).
- [25] Z. Nagy-Ungvarai, J. Ungvarai, and S. C. Müller, Complexity in spiral wave dynamics, *Chaos* **3**, 15 (1993).
- [26] G. Li, Q. Ouyang, V. Petrov, and H. L. Swinney, Transition from Simple Rotating Chemical Spirals to Meandering and Traveling Spirals, *Phys. Rev. Lett.* **77**, 2105 (1996).
- [27] Z. Qu, J. N. Weiss, and A. Garfinkel, Spatiotemporal Chaos in a Simulated Ring of Cardiac Cells, *Phys. Rev. Lett.* **78**, 1387 (1997).
- [28] M. Courtemanche, J. P. Keener, and L. Glass, A delay equation representation of pulse circulation on a ring in excitable media, *SIAM J. Appl. Math.* **56**, 119 (1996).
- [29] R. J. Adrian, K. T. Christensen, and Z.-C. Liu, Analysis and interpretation of instantaneous turbulent velocity fields, *Exp. Fluids* **29**, 275 (2000).
- [30] P. Wassermann and M. Kloker, Transition mechanisms induced by travelling crossflow vortices in a three-dimensional boundary layer, *J. Fluid Mech.* **483**, 67 (2003).

- [31] Y. Wang and L. Bourouiba, Non-Galilean Taylor-Culick law governs sheet dynamics in unsteady fragmentation, *J. Fluid Mech.* (to be published).
- [32] G. Gerber, D. A. Weitz, and P. Coussot, Propagation and adsorption of nanoparticles in porous medium as traveling waves, *Phys. Rev. Research* **2**, 033074 (2020).
- [33] T. R. Salamon, R. C. Armstrong, and R. A. Brown, Traveling waves on vertical films: Numerical analysis using the finite element method, *Phys. Fluids* **6**, 2202 (1994).
- [34] B. J. Matkowsky and G. I. Sivashinsky, Acceleration effects on the stability of flame propagation, *SIAM J. Appl. Math.* **37**, 669 (1979).
- [35] A. Saha, N. Pal, and P. Chatterjee, Dynamic behavior of ion acoustic waves in electron-positron-ion magnetoplasmas with superthermal electrons and positrons, *Phys. Plasmas* **21**, 102101 (2014).
- [36] J. J. Tyson and J. P. Keener, Singular perturbation theory of traveling waves in excitable media (A review), *Physica D* **32**, 327 (1988).
- [37] J. D. Murray, E. A. Stanley, and D. L. Brown, On the spatial spread of rabies among foxes, *Proc. R. Soc. London, Ser. B* **229**, 111 (1986).
- [38] G. Abramson, V. M. Kenkre, T. L. Yates, and R. R. Parmenter, Traveling waves of infection in the hantavirus epidemics, *Bull. Math. Biol.* **65**, 519 (2003).
- [39] J. P. Lu and J. L. Birman, Acoustic-wave propagation in quasiperiodic, incommensurate, and random systems, *Phys. Rev. B* **38**, 8067 (1988).
- [40] H. R. Brand and R. J. Deissler, Transition from propagating localized states to spatiotemporal chaos in phase dynamics, *Phys. Rev. E* **58**, R4064(R) (1998).
- [41] Here, we use “quasiperiodic” in the context that it has come to be used in applications, namely to describe a function of time depending only on periodic functions collectively having incommensurable temporal periods, cf. D. D. Joseph, *Stability of Fluid Motions* (Springer, New York, 1976), Vol. I, p. 58. We use “quasiperiodicity” in a similar way.
- [42] W. D. Caraway IV, Analysis of a partial differential equation related to pressure-driven separations of binary liquids, M.S. thesis, University of Illinois at Urbana-Champaign (2020).
- [43] See Supplemental Material at <http://link.aps.org/supplemental/10.1103/PhysRevE.106.024607>, which includes Ref. [49].
- [44] T. Pezeril, G. Saini, D. Veysset, S. Kooi, P. Fidkowski, R. Radovitzky, and K. A. Nelson, Direct Visualization of Laser-Driven Focusing Shock Waves, *Phys. Rev. Lett.* **106**, 214503 (2011).
- [45] C. J. Elkins and M. T. Alley, Magnetic resonance velocimetry: Applications of magnetic resonance imaging in the measurement of fluid motion, *Exp. Fluids* **43**, 823 (2007).
- [46] D. S. Ching, C. J. Elkins, M. T. Alley, and J. K. Eaton, Unsteady vortex structures in the wake of nonaxisymmetric bumps using spiral MRV, *Exp. Fluids* **59**, 144 (2018).
- [47] P. J. Mulholland *et al.*, Nitrogen cycling in a forest stream determined by a ^{15}N tracer addition, *Ecol. Monogr.* **70**, 471 (2000).
- [48] C. A. Misretta, Sub-Nyquist acquisition and constrained reconstruction in time resolved angiography, *Med. Phys.* **38**, 2975 (2011).
- [49] H. P. Manning, *Geometry of Four Dimensions* (Macmillan, New York, 1914).
- [50] J. Koch, M. Kurosaka, C. Knowlen, and J. Kutz, Multiscale physics of rotating detonation waves: Autosolitons and modulational instabilities, *Phys. Rev. E* **104**, 024210 (2021).
- [51] F. Feudel, N. Seehafer, B. Galanti, and S. Rüdiger, Symmetry-breaking bifurcations for the magnetohydrodynamic equations with helical forcing, *Phys. Rev. E* **54**, 2589 (1996).
- [52] Y. Shen, P. F. Chen, Y. D. Liu, K. Shibata, Z. Tang, and Y. Liu, First unambiguous imaging of large-scale quasi-periodic extreme-ultraviolet wave or shock, *Astrophys. J.* **873**, 22 (2019).
- [53] F. T. M. Nguyen and M. D. Graham, Buckling instabilities and complex trajectories in a simple model of uniflagellar bacteria, *Biophys. J.* **112**, 1010 (2017).
- [54] B. Pier, Periodic and quasiperiodic vortex shedding in the wake of a rotating sphere, *J. Fluids Struct.* **41**, 43 (2013).
- [55] R. Paccagnella, Pressure-driven reconnection and quasi-periodical oscillations in plasmas, *Phys. Plasmas* **21**, 032307 (2014).
- [56] G. Sivashinsky, On spinning propagation of combustion waves, *SIAM J. Appl. Math.* **40**, 432 (1981).
- [57] R. A. Waldron, A helical coordinate system and its applications in electromagnetic theory, *Q. J. Mech. Appl. Math.* **11**, 438 (1958).
- [58] P. J. Lin-Chung and A. K. Rajagopal, Helical coordinate system and electrostatic fields of double-helix charge distributions, *Phys. Rev. E* **52**, 901 (1995).
- [59] G. M. Webb, C. M. Ko, G. P. Zank, and J. R. Jokipii, Diffusive-compression acceleration and turbulent diffusion of cosmic rays in quasi-periodic and turbulent flows, *Astrophys. J.* **595**, 195 (2003).
- [60] P. Grassberger and I. Procaccia, Characterization of Strange Attractors, *Phys. Rev. Lett.* **50**, 346 (1983).